NJC

Accepted Manuscript

This is an *Accepted Manuscript*, which has been through the Royal Society of Chemistry peer review process and has been accepted for publication.

Accepted Manuscripts are published online shortly after acceptance, before technical editing, formatting and proof reading. Using this free service, authors can make their results available to the community, in citable form, before we publish the edited article. We will replace this *Accepted Manuscript* with the edited and formatted *Advance Article* as soon as it is available.

You can find more information about *Accepted Manuscripts* in the Information for Authors.

Please note that technical editing may introduce minor changes to the text and/or graphics, which may alter content. The journal's standard Terms & Conditions and the Ethical guidelines still apply. In no event shall the Royal Society of Chemistry be held responsible for any errors or omissions in this *Accepted Manuscript* or any consequences arising from the use of any information it contains.

ROYAL SOCIETY OF CHEMISTRY

www.rsc.org/njc

DNA-binding studies and antioxidant activities of two-, three- and four-coordinate silver(I) complexes containing bis(2-benzimidazolyl)aniline derivatives

Huilu Wu*, Yanhui Zhang, Chengyong Chen, Jiawen Zhang, Yuchen Bai, Furong Shi and Xiaoli Wang

School of Chemical and Biological Engineering, Lanzhou Jiaotong University, Lanzhou 730070, P. R. China.

Abstract: Three ligands bis(benzimidazol-2-ylmethyl)aniline (bba), bis(*N*-methylbenzimidazol-2-ylmethyl)aniline (Mebba), and bis(N-ethylbenzimidazol-2-ylmethyl)aniline (Etbba) have been prepared. Reaction of these shape-specific designed ligands with Ag(pic) (pic = picrate) afforded three novel complexes, namely, $[Ag_2(bba)_2](pic)_2 \cdot 2DMF$ **1**, $[Ag(Mebba)_2](pic) \cdot Et_2O$ **2** and [Ag(Etbba)(pic)] **3**. The ligands and Ag(I) complexes were characterized by elemental analysis, UV-Vis, IR, NMR and X-ray crystallography. **1** is a dinuclear metallacycle with 2-fold rotational symmetry in which two *syn*-conformational bba ligands are connected by two linearly coordinated Ag(I) atoms. **2** consists of a centrosymmetric uninuclear pore canal structure assembled from a Ag(I) ions and two Mebba ligands, resulting in a distorted tetrahedron geometry. The structure of **3** consists of a ligand of the Etbba, one picrate, and one Ag(I) atom, and the coordination geometry around Ag(I) is best described as Y-shaped. In order to explore the relationship between the structure and biological properties, the DNA-binding properties have been investigated by electronic absorption, fluorescence, and viscosity measurements. The experimental results suggest that Ag(I) complexes bind to DNA in an intercalation mode, and their binding affinity for DNA follows the order **2** > **1** > **3.**

* Corresponding author. *Tel*: +86 13893117544.
E-mail:wuhuilu@163.com. (H. L. Wu)

Moreover, antioxidant activities of the title complexes have been investigated. The result demonstrates that the three Ag(I) complexes have a strong potential to be applied as scavengers to eliminate hydroxyl and superoxide radicals in *vitro* studies.

Introduction

DNA is generally the primary intracellular target of anticancer drugs. The interaction between small molecules and DNA can often cause DNA damage in cancer cells, blocking the division of cancer cells and resulting in cell death.[1, 2] Transition metal complexes are used to bind and react at specific sequences of DNA for finding novel chemotherapeutics, probing DNA and developing highly sensitive diagnostic agents.[3, 4] The complexes have been extensively utilized in metal-mediated DNA cleavage for the generation of activated oxygen species. Therefore, the research on the mechanism of the interaction of complexes with DNA is attracting more and more attention. The results will potentially be useful in the design of new compounds that can recognize specific sites or conformations of DNA.[5, 6] Furthermore, silver complexes have showed anti-HIV activities. For this reason, a number of silver complexes were screened for anticancer activity and some of them were found active both *in vivo and in vitro*.[7]

N-heterocyclic carbenes (NHCs), commonly derived from benzimidazolium (imidazolium) salts, have attracted widespread attention as ligands for transition metals and main group elements.[8, 9] A variety of related metal complexes have been synthesized through deprotonation of N, N-disubstituted imidazolium salts.[10-13] NHC silver complexes have played an important role in the rapid development of NHC metal complexes.[14-16] One reason for this is that NHC silver complexes are easily prepared by a one-pot reaction of an benzimidazolium (or imidazolium) salt with Ag_2O, which can be easily derived. Another reason for this is that carbene silver complexes can be used as carbene transfer reagent for synthesis of Ni, Pd, Pt, Cu, Au, Rh, Ir and Ru carbene complexes, such a route affords a convenient method for the preparation of these carbene metal complexes.[17] In addition, A new discovery shows

that Ag(I)–carbene complexes have shown interesting biological activity as antimicrobial and antimitochondrial agents, respectively.[18, 19]

Interests in bis(2-benzimidazolyl)aniline and their derivatives are widespread. In our previous work, we have investigated the coordinating ability of some kind of benzimidazole ligands and their complexes.[7, 19] In this paper, we wish to report the synthesis, structure, DNA-binding activities and antioxidant activity of the Ag(I) complex **1**-**3**. These new complexes are of interest as potential precursors for NHC complexes of other transition metals.

Results and Discussion

The Ag(I) complexes were prepared by reaction of Ag(pic) with three ligands bba, Mebba and Etbba in methanol, respectively. Synthetic routes of ligands and Ag(I) complexes are shown in Scheme 1. The three ligands and their Ag(I) complexes are very stable in atmospheric condition. They are soluble in polar aprotic solvents such as DMF, DMSO and CH_3CN, slightly soluble in ethanol, ethyl acetate and chloroform, and insoluble in water, Et_2O and petroleum ether. The elemental analyses show that their different compositions.

[Insert Scheme 1]

IR and UV spectra

The IR spectral data for the free ligands and Ag(I) complexes with their relative assignments have been studied to characterize their structures. The IR spectra of complex **1** are closely related to that of the free ligand bba. The spectrum of bba shows a strong band at 1445 cm^{-1} and weak bands at 1610 cm^{-1}. By analogy with the assigned bands of imidazole, the two bands are attributed to the ν(C=N) and ν(C=C) frequencies of the benzimidazole group, respectively.[20-22] The location of the two bands was slightly shifted for complex **1**, one shift around 10 cm^{-1} and another around 5 cm^{-1} in the complexes, which can be attributed to the coordination of the benzimidazole nitrogen to the metal center atom.[23] Similar shifts also appear in

complexes **2** and **3**, which gives the same conclusion. Moreover, information regarding the possible bonding modes of the picrate and benzimidazole rings may also be obtained from the IR spectra.[24]

DMF solutions of ligands and Ag(I) complexes show, as expected, almost identical UV spectra. The UV bands of bba (277, 282 nm) are only marginally red-shifted about 3 nm for complex **1**, which is evidence of C=N coordination to the metal center. These bands are assigned to n→π* and π→π* (imidazole) transitions. Analogously, the UV bands of Mebba (280, 286 nm), Etbba (280, 287 nm) are also marginally red-shifted about 3-4 nm in complexes **2** and **3**. This phenomenon also shows that C=N is involved in coordination to the metal center. The picrate bands (observed at 380 nm in the complexes) are assigned to π→π* transitions.[25]

Crystal structures

The X-ray single-crystal analyses suggest that structural diversification did occur in the process of coordination assembly, namely, different or isomeric structures were obtained from different ligands and silver ions.

Crystal Structure of complex 1. The crystal structure of **1** consists of a binuclear dicationic $[Ag_2(bba)_2]^{2+}$ motif and two picrate anions. Two ligands are arranged in a face-to-face *syn*-conformation to coordinate to two Ag(I) ions from opposite directions, generating a locally linear geometry around the metal ions. The metallacycle exhibits an overall chairlike conformation possessing a crystallographically imposed inversion center. Each silver(I) ion is coordinated to two imidazole N donors, with the N-Ag-N bond angles close to linearity (N(5)-Ag(1)-N(3)#1, 171.67°). The Ag(1)···Ag(1A) distance (4.611 Å) is much longer than the upper limit (2.91-3.24 Å) of those reported for weak Ag···Ag interaction in other silver(I) complexes.[26-28] This leads to the formation of a typical rectangular cavity formed from two ligands and two silver(I) ions, The picrate anions do not participate in the coordination and only act as counter anions for charge equilibrium.(Fig.1)

[Insert Fig.1]

As shown in Fig. 2, benzene ring from neighboring picrate anions are in parallel position by the $\pi\cdots\pi$ interactions (centroid-to-centroid distances: 3.559 Å) and two adjacent picrate anions are inlaid in the coordination cations as a sandwich and are together by the $\pi\cdots\pi$ interactions (centroid-to-centroid distances: 3.474 Å), so the geometry of the complex ion is propagated into an infinite 1-D chain. In addition, because of the existence of the solvated DMF molecules, which form C-H···O hydrogen bonds (C-O 2.642-3.425 Å and C-H-O 99.8-165.4°) and N-H···N hydrogen bonds (N-N 3.261 Å and N-H-N 91.8°) with the anions.[29] Such arrangement can make the crystal structure more stable.

[Insert Fig.2]

Crystallographic analysis reveals that complex **1** is a 3D structure due to coordination of binuclear dicationic $[Ag_2(bba)_2]^{2+}$ motif.[30] The coordination geometry of Ag(I) ion with two N donors from two bba ligands (Figure 3a). The shortest Ag(I)···Ag(I)distance along the silver chain is 2.91 Å, and the shortest Ag(I)···Ag(I) distance between two adjacent silver chains is 4.611 Å. Formation of 3D structure prevents the non-coordinating N atoms from forming hydrogen bonds. In Fig 3, the $[Ag_2(bba)_2]^{2+}$ units are arranged such that differently sized channels originating from inner cavities can be observed in all directions (Figure 3a and 3b).

[Insert Fig.3]

Crystal Structure of complex 2. The single-crystal X-ray structure of complex **2** revealed that Ag(I) center is four-coordinated distorted tetrahedron, which is coordinated by through four benzimidazole nitrogen atoms(Ag-N bond between 2.285 and 2.341 Å) from two Mebba ligands(Fig. 4a). The ligand–metal–ligand angles vary from 97.45(8)° [N(8)-Ag(1)-N(10)] to 132.95(19)° [C(8)-N(3)-Ag(1)]. Besides, the largest dihedral angle between planes N(3)-Ag-N(10) and N(3)-Ag-N(5) is 73.1°, while the smallest dihedral angle between planes N(5)-Ag-N(10) and N(8)-Ag-N(10) is 34.79°. So the environment of the Ag(I) ion may be treated as a distorted tetrahedron (Fig. 4b). Owing to this coordination geometry, a 8-membered ring was

constructed, which connected through the Ag(I) centers and displaying an 8-shaped geometry (Fig. 4c).[31]

[Insert Fig.4]

The $\pi\cdots\pi$ interactions between two benzimidazole rings (centroid to-centroid distances: 3.486 and 3.763 Å) in complex **2** also link the dimeric cations, extending into a 2D structure in the *ac* plane (Figure 5 in the Supporting Information). Neighboring chains are connected by C-H···O hydrogen bonds(C-O 3.151-3.462 Å), thus generating an infinite 2-D layer.[32]

[Insert Fig.5]

Crystal Structure of complex 3. The ORTEP structure of complex **3** with atom labeling is shown in Fig.6. The molecular structure consists of a ligand of the Etbba, one picrate anion, and one Ag(I) atom. The central Ag(I) is three coordinated by one O atom (d_{Ag-O} = 2.468 (3)) from picrate anion , Two benzimidazole N atom (d_{Ag-N} = 2.256(3) and 2.197(3)) from Etbba ligand, and the ligand–metal–ligand angles vary from 92.18° to 141.60°, so the coordination geometry around Ag(I) is best described as Y-shaped.[33, 34] In addition, picrate group and Etbba ligand show weak coordination to Ag(I) in the chelated mode with the Ag-O(7) and Ag-N(1) distances of 2.769(4) and 2.840(3) Å. As shown in Fig. 6.

[Insert Fig.6]

As one of important types of supramolecular forces, $\pi\cdots\pi$ stacking shows a specific structural requirement for substrate recognition or the arrangement of complicated architectures. In complex **3**, the centroid-to-centroid distance of 3.499 Å between the two nearly parallel planes of the benzimidazole ring of one ligand and benzene ring of picrate anion indicates strong intramolecular interactions. The 2D structure was formed through $\pi\cdots\pi$ interactions and weak C-O···H hydrogen bonding (C-O 2.648-3.471 Å and C-H-O 100.3-160.2°) between benzimidazole and picrate anion in adjacent chains (Figure 7).[35]

[Insert Fig.7]

From the above crystal structures of three Ag(I) complexes, the cation of the complex **1** can be described as an overall chairlike conformation possessing a crystallographically imposed inversion center, the geometric structure of **2** may be treated as a distorted tetrahedron, the coordinate form of the complex **3** can be described as Y-shaped. By comparison of the molecular structure of Ag(I) complexes, we have found that their structural conformations were mainly controlled by the ligands and metal centers, and also influenced by the coordination capabilities of counter anions at the same time. The intramolecular weak interactions also help to assemble the crystal structures into different dimensions.

DNA Binding Properties

DNA binding is a critical step for subsequent cleavage. Therefore, prior to investigation of the nuclease activities of **1-3** complexes, the binding properties of the Ag(I) species with DNA were examined using various techniques.

UV/Vis Absorption Studies. The absorption titration experiment was carried out to investigate the binding affinity of the Ag(I) complexes with CT-DNA. Complex binding with DNA via intercalation generally results in hypochromism and a red shift (bathochromism) of the absorption band due to a strong stacking interaction between an aromatic moiety of the ligand and the base pairs of the DNA.[36, 37] On the other hand, the absorption intensity of a complex is increased (hyperchromism) upon increasing the concentration of CT-DNA owing to the degradation of the DNA double-helix structure.[38] The extent of the hyperchromism is indicative of the partial or non-intercalative binding modes, such as electrostatic forces, van der Waals interactions, dative bonds, hydrogen bonds and hydrophobic interactions

The absorption spectra of **1-3** complexes in the absence and presence of CT-DNA (at a constant concentration of complexes) are given in Fig. 8, respectively. As can be seen from Fig. 8, the **1-3** complexes exhibit intense absorption bands at 281-283 nm assigned to $\pi \rightarrow \pi^*$ transition of the benzimidazole, and addition of increasing amounts of CT-DNA results in hypochromism and bathocromic shift in the UV-vis spectra of the compounds. In the present case, with addition of DNA, the Ag(I)

complexes exhibit hypochromism of about 28.5%, 46.8% and 57.0% accompanied by bathochromism about 1-2 nm shift in the absorption maxima. The spectroscopic changes suggest that the Ag(I) complexes have stronger interaction with DNA.

The intrinsic binding constants K_b of the Ag(I) complexes were 4.85×10^4 M^{-1} (R^2 = 0.9889 for 16 points), 1.51×10^5 M^{-1} (R^2 = 0.9889 for 16 points) and 3.56×10^4 M^{-1} (R^2 =0.9889 for 16 points), respectively. Compared with those of so-called DNA-intercalative lutetium complexes (5.3×10^3-2.3×10^4 M^{-1}),[39] the binding constants (K_b) of the Ag(I) complexes can suggest that three Ag(I) complexes most possibly bind to DNA in an intercalation mode. So, from the above intrinsic binding constant values, it indicates that the binding affinity of the Ag(I) complexes is **2** > **1** > **3**. This may be attributed to three possible reasons: i) This difference of the ligands and Ag(I) complexes in DNA binding ability could be attributed to the presence of an electron deficient center in the charged Ag(I) complexes where an additional interaction between the complex and phosphate-rich DNA backbone may take place.[40, 41] ii) By comparison of their molecular structures, we find the greater number of coplanar aromatic rings, which contribute to intercalation to the base pairs of double helical DNA, may result stronger affinity for DNA.[7, 25] iii) The charge transfer of coordinated ligands caused by the coordination of the silver atom, result in the decline of the charge density of the plane conjugate system, which contribute to insert.[19, 42] This result further illustrates that electron density and steric hindrance play a very important role in the DNA-binding of three Ag(I) complexes.

[Insert Fig.8]

Fluorescence spectroscopic studies. In order to test whether the complexes can bind to DNA by the mode of intercalation, competitive EB binding studies were undertaken to gain supports for the above spectral result. EB was employed since EB interacts with DNA as a typical indicator of intercalation.[43] If a complex can replace EB from DNA-bound EB, the fluorescence of the solution will be quenched due to the fact that free EB molecules are readily quenched by the surrounding water molecules.[44] For all the complexes, no emission was observed either alone or in the

presence of CT-DNA in the buffer. The fluorescence quenching of EB bound to CT-DNA by complexes **1-3** are shown in Fig. 9. The quenching of EB bound to CT-DNA by three Ag(I) complexes are in good agreement with the linear Stern–Volmer equation, which provides further evidence that the Ag(I) complexes bind to DNA and only one type of quenching process occurs. The K_{sv} values for complexes **1-3** are 3.65×10^2 M^{-1} (R^2 = 0.9984 for 16 points), 4.11×10^2 M^{-1} (R^2 = 0.99755 for 16 points) and 3.2×10^2 M^{-1} (R^2 = 0.9709 for 11 points), respectively. The Stern–Volmer dynamic quenching constants can also be interpreted as binding affinities of the complexation reactions.[45, 46] The data of K_{sv} present the order **2** > **1** > **3** for complexes, which indicate the abilities of displacement of EtBr from EtBr–DNA systems by compounds and the binding affinities between compounds and DNA, which is consistent with absorption spectral results.

[Insert Fig.9]

Viscosity titration measurements. Photophysical experiments provide necessary, but not sufficient clues to support a binding mode. Measurements of DNA viscosity that is sensitive to DNA length change are regarded as the least ambiguous and the most critical tests of binding in solution in the absence of crystallographic structural data.[47, 48] A classical intercalation model results in lengthening of the DNA helix as base pairs are separated to accommodate the binding reagent, leading to the increase of DNA viscosity. In contrast, a partial and/or non-classical intercalation could bend or kink the DNA helix, reduce its effective length and, concomitantly, its viscosity. The effects of the Ag(I) complexes on the viscosities of CT-DNA are shown in Fig. 10. With the ratios of the investigated complexes to DNA increase, the relative viscosities of DNA increase steadily, and almost at the same magnitude of change, indicating that there exist intercalations between all the complex with DNA helix. For the three complexes, though the results certified they all bind to DNA via an intercalation binding mode, the different on the magnitude of change suggested the extents of the unwinding and lengthening of DNA helix by those and the affinities binding to DNA as follow the order of **2** > **1** >**3**. So the results demonstrate that the complex could

bind to DNA by intercalation mode, which is consistent with the above absorption and fluorescence spectral results.

[Insert Fig.10]

Antioxidant activities

Generation of reactive oxygen species (ROS) is a normal process in the life of aerobic organisms. $OH^{-\bullet}$ and $O_2^{-\bullet}$ are two clinically important reactive oxygen species in the human body.[49] They are produced in most organ systems and participate in various physiological and pathophysiological processes such as carcinogenesis, aging, viral infection, inflammation and others.[50] We therefore also conducted an investigation to explore whether the Ag(I) complexes have the antioxidant activities.

Hydroxyl radical scavenging activity. We compared the abilities of the Ag(I) complexes to scavenge hydroxyl radicals with those of the well-known natural antioxidants mannitol and vitamin C, using the same method as reported in a previous paper.[7, 51] The 50% inhibitory concentration (IC_{50}) value of mannitol and vitamin C are about 9.6×10^{-3} and 8.7×10^{-3} M, respectively. Fig. 11 shows the plots of hydroxyl radical scavenging effect (%) for the Ag(I) complexes, respectively, the IC_{50} values of complexes **1**, **2** and **3** are 5.08×10^{-5} M, 3.95×10^{-5} M and 5.67×10^{-5} M, respectively, which implies that the three Ag(I) complexes exhibits better scavenging activity than mannitol and vitamin C. It can be concluded that a much less or no scavenging activity was exhibited by the free ligands when compared to that of Ag(I) complexes which is due to the chelation of ligand with the central metal atom.[7] The lower IC_{50} values observed in antioxidant assays did demonstrate that the three Ag(I) complexes have a strong potential to be applied as scavengers to eliminate radicals.

[Insert Fig.11]

Superoxide radical scavenging activity. As another assay of antioxidant activity, superoxide radical ($O_2^{-\bullet}$)-scavenging activity has been investigated.[39] Complexes **1** and **2** have good superoxide radical scavenging activity, but complex **3** does not have the activity. As shown in Fig. 12, the IC_{50} value of complex **1** and **2** are 1.53×10^{-3} M

and 2.4× 10^{-3} M, which indicates that complexes **1** and **2** exhibit good superoxide radical-scavenging activity and may be an inhibitor (or a drug) to scavenge superoxide radical ($O_2^{-\bullet}$) in *vivo* which need further investigation.

[Insert Fig.12]

Conclusions

In this paper, The bis-benzimidazole ligands and their Ag(I) complexes have been synthesized and characterized. The cation of the complex **1** can be described as an overall chairlike conformation possessing a crystallographically imposed inversion center, owing to the strong interactions between the two Ag(I) ions themselves. The geometric structure of **2** may be treated as a distorted tetrahedron. In the complex **3,** the coordination geometry around Ag(I) is best described as Y-shaped. DNA-binding of the Ag(I) complexes suggest that the three ligands and Ag(I) complexes bind to DNA in an intercalation mode, which is due to the large planar aromatic rings, hydrogen bonds and π···π stacking interactions that facilitate them intercalating into the base pairs of double helical DNA. The DNA-binding affinities of these three complexes follow the order **2** > **1** > **3**. Furthermore, the Ag(I) complexes have stronger ability of antioxidation for hydroxyl radical and superoxide radical. These findings indicate that Ag(I) complexes have potential practical applications in the development of potential probes of DNA structure and conformation and new therapeutic reagents for diseases on the molecular level, which warrants further *in vivo* experiments and pharmacological assays.

Experimental

General methods

All chemicals and solvents were reagent grade and were used without further purification. The C, H and N elemental analyses were determined using a Carlo Erba 1106 elemental analyzer. The IR spectra were recorded in the 4000–400 cm^{-1} region with a Nicolet FT-VERTEX 70 spectrometer using KBr pellets. Electronic spectra were taken on a Lab-Tech UV Bluestar spectrophotometer. The absorbance was

measured with Spectrumlab 722sp spectrophotometer at room temperature. ^{1}H-NMR spectra were recorded on a Varian VR300-MHz spectrometer with TMS as an internal standard. Electrolytic conductance measurements were made with a DDS-307 type conductivity bridge using 3×10^{-3} M solutions in DMF at room temperature.

Synthesis of the ligand and silver complexes

Synthesis of bba and Etbba. The ligands bba and Etbba were synthesized according to the procedure reported in Ref.[52, 53]

Synthesis of Mebba. 5.3 g (0.015 mol) bis(benzimidazol-2-ylmethyl)aniline(bba) with 1.17 g (0.03 mol) potassium in 150 mL evaporated tetrahydrofuran was followed by adding 4.26 g (0.03 mol) iodomethane. The resulting solution was concentrated and recrystallized from methanol which was given pale yellow block crystals of Mebba. Yield : 62%, m.p: 236-238°C. Elemental analysis for $C_{24}H_{23}N_5$: calculated(%): C, 75.56; H, 6.08; N, 18.36. Found(%): C, 75.53; H, 6.10; N, 18.37. IR (KBr; ν/cm^{-1}): 744 ν(o-Ar), 1278 ν(C-N), 1467 ν(C=N), 1604 ν(C=C). ^{1}H NMR (400 MHz, [D6]DMSO): δ = 7.13-7.60(m, 8H, benzimidazole), 7.09-6.64(m, 5H, Ph), 5.019(s, 4H, CH_2), 3.78(s, 6H, CH_3). UV-Visible (in DMF), λ_{max} (nm): 280 and 286.

Preparation of complexes. To a stirred solution of Ligand bba (176.7 mg, 0.50 mmol) in hot MeOH (10 mL) was added Ag(pic) (170.0 mg, 0.50 mmol) in MeOH (5 mL). A yellow crystalline product formed rapidly. The precipitate was filtered off, washed with MeOH and absolute Et_2O, and dried in *vacuo*. The dried precipitate was dissolved in DMF to form a yellow solution into which Et_2O was allowed to diffuse in at room temp. Crystals suitable for X-ray measurement were obtained after several days. Complexes **2** and **3** were prepared by a similar procedure as for complex **1**.

1, Yield: 52%. Elemental analysis for $C_{62}H_{56}Ag_2N_{18}O_{16}$: calculated(%): C, 48.83; H, 3.7; N, 16.53. Found (%): C, 48.85; H, 3.68; N, 16.54. IR (KBr; ν/cm^{-1}): 743 ν (*o*-Ar), 1273 ν(C-N), 1365 ν(O-N-O), 1456 ν(C=N), 1612 ν(C=C). UV-Visible (in DMF), λ_{max} (nm): 276, 282 and 380.

2, Yield: 59%. Elemental analysis for $C_{58}H_{58}AgN_{13}O_8$: calculated(%): C, 59.39; H, 4.98; N, 15.52. Found(%): C, 59.37; H, 4.99; N, 15.53. IR (KBr; ν/cm^{-1}): 743 ν (*o*-Ar),

1266 *v*(C-N), 1365 *v*(O-N-O), 1456 *v*(C=N), 1637 *v*(C=C). UV-Visible (in DMF), λ_{max} (nm): 277, 283 and 380.

3, Yield: 75%. Elemental analysis for $C_{32}H_{29}AgN_8O_7$: calculated(%):C, 51.56 H, 3.92; N, 15.03. Found(%): C, 51.57, H, 3.91; N, 15.05. IR (KBr; *v*/cm^{-1}): 746 *v* (*o*-Ar), 1266 *v*(C-N), 1363 *v*(O-N-O), 1453 *v*(C=N) , 1615 *v*(C=C). UV-Visible (in DMF), λ_{max} (nm): 276, 283 and 380.

X-ray crystallography

Suitable single crystals were mounted on a glass fiber, and the intensity data were collected on a Bruker APEX II area detector with graphite-monochromated Mo-K_α radiation (λ= 0.71073Å) at 296(2) K. Data reduction and cell refinement were performed using the SMART and SAINT programs. The absorption corrections are carried out by the empirical method. The structure was solved by direct methods and refined by full-matrix least-squares against F^2 of data using SHELXTL software.[54] All H atoms attached to C atoms except for DMF and diethyl ether groups were fixed geometrically and treated as riding with C-H = 0.93 or 0.97 Å with U_{iso}(H) = 1.2U_{eq}(C). All H atoms attached to N atoms were fixed geometrically and treated as riding with N-H =0.86 Å with U_{iso}(H) = 1.2U_{eq}(N). H atoms attached to C atoms at DMF and diethyl ether groups were also calculated geometrically and included into the refinement with C-H = 0.96 Å, U_{iso}(H) = 1.5U_{eq}(C). Basic crystal data, description of the diffraction experiment, and details of the structure refinement are given in Table 1. Selected bond distances and angles are presented in Table 2.

Table 1. Crystal and structure refinement data for complexes **1**, **2** and **3**

Complex	**1**	**2**	**3**
Empirical formula	C_{62} H_{56} Ag_2 N_{18} O_{16}	C_{58} H_{58} Ag N_{13} O_8	C_{32} H_{29} Ag N_8 O_7
Molecular weight	1524.99	1173.04	745.50
Crystal system	Triclinic	Triclinic	Orthorhombic
Space group	P-1	P-1	P2(1)2(1)2(1)
a (Å)	9.5997(12)	14.0351(16)	6.951(4)
b (Å)	10.9697(15)	15.1423(12)	17.701(9)
c (Å)	15.236(2)	15.6532(18)	24.901(13)
α (°)	99.118(2)	106.739(8)	90

β (°)	96.954(2)	116.2520(10)	90
γ (°)	94.303(2)	98.591(7)	90
V (Å^3)	1565.2(4)	2704.7(5)	3064(3)
Z, Dc (mg/m^3)	1, 1.618	2, 1.440	4, 1.616
μ (mm^{-1})	0.712	0.442	0.722
F (000)	776	1216	1520
θ range for data collection(°)	2.99 – 25.49	1.48 – 25.50	2.30 – 25.50
Crystal size(mm)	0.40 x 0.38 x 0.30	0.40 x 0.38 x 0.30	0.40 x 0.38 x 0.30
Limiting indices, *h k l*	-11 to 11	-16 to 16	-8 to 4
	-13 to 13	-18 to 17	-21 to 20
	-18 to 18	-18 to 18	-29 to 30
Reflections collected	12722	19886	14493
Unique reflections	5736	9899	5694
R_{int}	0.0342	0.0241	0. 0221
Data / restraints / parameters	5736 / 12/ 445	9899 / 6 / 727	5694 / 19 / 435
Goodness-of-fit on F^2	1.096	1.038	1.053
R_1/wR_2 [$I > 2\sigma(I)$]	0.0359 / 0.0984	0.0370 / 0.0985	0.0330/ 0.0721
R_1/wR_2 (all data)	0.0400 / 0.1053	0.0478 / 0.1060	0.0401 / 0.0756
Largest diff. peak, hole (e Å^{-3})	0.746, -0.600	0.777, -0.530	0.496, -0.872

Table 2. Selected bond distances (Å) and angles (°) for complexes **1**, **2** and **3**.

Complex **1**			
Ag(1)-N(5)	2.116(2)	Ag(1)-N(3)#1	2.118(2)
N(3)-Ag(1)#1	2.118(2)		
N(5)-Ag(1)-N(3)#1	171.67(10)	C(16)-N(3)-Ag(1)#1	129.8(2)
C(22)-N(3)-Ag(1)#1	124.3(2)	C(1)-N(5)-Ag(1)	125.3(2)
C(7)-N(5)-Ag(1)	128.4(2)		
Complex **2**			
Ag(1)-N(5)	2.285(2)	Ag(1)-N(8)	2.317(2)
Ag(1)-N(10)	2.337(2)	Ag(1)-N(3)	2.341(2)
N(5)-Ag(1)-N(8)	117.60(8)	N(5)-Ag(1)-N(10)	120.66(8)
N(8)-Ag(1)-N(10)	97.45(8)	N(5)-Ag(1)-N(3)	103.71(8)
N(8)-Ag(1)-N(3)	111.84(8)	N(10)-Ag(1)-N(3)	105.20(8)
C(8)-N(3)-Ag(1)	132.95(19)	C(15)-N(3)-Ag(1)	120.99(18)
C(17)-N(5)-Ag(1)	125.06(18)	C(24)-N(5)-Ag(1)	127.43(19)
C(32)-N(8)-Ag(1)	126.9(2)	C(39)-N(8)-Ag(1)	127.6(19)
C(41)-N(10)-Ag(1)	130.76(19)	C(48)-N(10)-Ag(1)	118.15(18)
Complex **3**			
Ag-N(4)	2.197(3)	Ag-N(2)	2.256(3)
Ag-O(1)	2.468(3)	Ag-O(7)	2.769(4)
Ag-N(1)	2.840(3)		
N(4)-Ag-O(1)	141.60(10)	N(2)-Ag-O(1)	92.18(10)
N(4)-Ag-O(7)	101.40(10)	N(2)-Ag-O(7)	133.43(10)

O(1)-Ag-O(7)	62.55(10)	N(4)-Ag-N(1)	69.32(9)
N(2)-Ag-N(1)	69.41(9)	O(1)-Ag-N(1)	107.99(8)
O(7)-Ag-N(1)	152.48(11)	C(8)-N(4)-Ag	122.7(2)
C(17)-N(4)-Ag	131.5(2)	N(6)-O(7)-Ag	125.7(2)
N(4)-Ag-N(2)	119.85(11)	C(18)-N(2)-Ag	120.7(2)
C(26)-N(2)-Ag	129.5(2)		

Symmetry transformations used to generate equivalent atoms: #1 -x+1,-y,-z+1

DNA-binding studies by viscosity experiments， electronic absorption and fluorescence spectra

Viscosity experiments were conducted on an Ubbelodhe viscometer, immersed in a water bath maintained at 25.0 ± 0.1℃. Titrations were performed for the complexes (3-30 μM), and each compound was introduced into CT-DNA solution (42.5 μM) present in the viscometer. Data were presented as $(\eta/\eta_0)^{1/3}$ versus the ratio of the concentration of the compound to CT-DNA, where η is the viscosity of CT-DNA in the presence of the compound and η_0 is the viscosity of CT-DNA alone. Viscosity values were calculated from the observed flow time of CT-DNA-containing solutions corrected from the flow time of buffer alone (t_0), $\eta = (t - t_0)$.[55]

Absorption titration experiments were performed with fixed concentration of the complexes, while gradually increasing the concentration of CT-DNA. To obtain the absorption spectra, the required amount of CT-DNA was added to both compound solution and the reference solution to eliminate the absorbance of CT-DNA itself. From the absorption titration data, the binding constant (K_b) was determined using the equation:[50]

$$[DNA]/(\varepsilon_a-\varepsilon_f) = [DNA]/(\varepsilon_b-\varepsilon_f) + 1/K_b(\varepsilon_b-\varepsilon_f)$$

where [DNA] is the concentration of CT-DNA in base pairs, ε_a corresponds to the extinction coefficient observed (Aobsd/[M]), ε_f corresponds to the extinction coefficient of the free compound, ε_b is the extinction coefficient of the compound when fully bound to CT-DNA, and K_b is the intrinsic binding constant. The ratio of slope to intercept in the plot of $[DNA]/(\varepsilon_a-\varepsilon_f)$ versus [DNA] gave the value of K_b.

EB emits intense fluorescence in the presence of CT-DNA, due to its strong

intercalation between the adjacent CT-DNA base pairs. It was previously reported that the enhanced fluorescence can be quenched by the addition of a second molecule.[56, 57] The extent of fluorescence quenching of EB bound to CT-DNA can be used to determine the extent of binding between the second molecule and CT-DNA. The competitive binding experiments were carried out in the buffer by keeping [DNA]/[EB] = 1 and varying the concentrations of the compounds. The fluorescence spectra of EB were measured using an excitation wavelength of 520 nm, and the emission range was set between 550 and 750 nm. The spectra were analyzed according to the classical Stern–Volmer equation:[58]

$$I_0/I = 1 + K_{sv}[Q]$$

where I_0 and I are the fluorescence intensities at 599 nm in the absence and presence of the quencher, respectively, K_{sv} is the linear Stern–Volmer quenching constant, and [Q] is the concentration of the quencher. In these experiments [CT-DNA] = 2.5×10^{-3} mol/L, [EB] = 2.2×10^{-3} mol/L.

Antioxidant activities

Hydroxyl radical scavenging activity. Hydroxyl radicals were generated in aqueous media through the Fenton-type reaction.[50, 59] The reaction mixture (3 mL) contained 1.0 mL of 0.10 mmol aqueous safranin, 1 mL of 1.0 mmol aqueous EDTA–Fe(II), 1 mL of 3% aqueous H_2O_2, and a series of quantitative microadditions of solutions of the test compound. A sample without the tested compound was used as the control. The reaction mixtures were incubated at 37°C for 30 min in a water bath. The absorbance was then measured at 520 nm. All the tests were run in triplicate and are expressed as the mean and standard deviation (SD).The scavenging effect for $OH^{-\bullet}$ was calculated from the following expression:

$$\text{Scavenging effect (\%)} = (A_{\text{sample}} - A_{\text{blank}}) / (A_{\text{control}} - A_{\text{blank}}) \times 100$$

where A_{sample} is the absorbance of the sample in the presence of the tested compound, A_{blank} is the absorbance of the blank in the absence of the tested compound and A_{control} is the absorbance in the absence of the tested compound and EDTA–Fe(II).[60]

Superoxide radical-scavenging activity. A nonenzymatic system containing 1 mL

9.9×10^{-6} M $VitB_2$, 1 mL 1.38×10^{-4} M NBT, 1 mL 0.03 M MET was used to produce the superoxide anion ($O_2^{-\bullet}$), and the scavenging rate of $O_2^{-\bullet}$ under the influence of 0.1-1.0μM of the test compound was determined by monitoring the reduction in rate of transformation of NBT to monoformazan dye.[61] The solutions of MET, $VitB_2$ and NBT were prepared with 0.02 M phosphate buffer (pH=7.8) avoiding light. The reactions were monitored at 560 nm with a UV/Vis spectrophotometer, and the rate of absorption change was determined. The percentage inhibition of NBT reduction was calculated using the following equation:[62] percentage inhibition of NBT reduction= $(1-k'/k)\times100$, where k' and k present the slopes of the straight line of absorbance values as a function of time in the presence and absence of SOD mimic compound (SOD is superoxide dismutase), respectively. The IC_{50} values for the complexes were determined by plotting the graph of percentage inhibition of NBT reduction against the increase in the concentration of the complex. The concentration of the complex which causes 50% inhibition of NBT reduction is reported as IC_{50}.

Abbreviation

bba	bis(benzimidazol-2-ylmethyl)aniline
Mebba	bis(*N*-methylbenzimidazol-2-ylmethyl)aniline
Etbba	bis(N-ethylbenzimidazol-2-ylmethyl)aniline
MeOH	methanol
DMF	N, N-dimethylformamide
DMSO	dimethylsulphoxide
Et_2O	diethyl ether
SOD	superoxide dismutase

Acknowledgement

The present research was supported by the National Natural Science Foundation of China (Grant No. 21367017), the Fundamental Research Funds for the Gansu Province Universities (212086), Natural Science Foundation of Gansu Province

(Grant No. 1212RJZA037), and 'Qing Lan' Talent Engineering Funds for Lanzhou Jiaotong University.

Appendix A. Supplementary data

Crystallographic data for complexes **1**-**3** have been deposited with the Cambridge Crystallographic Data Centre as supplementary publication CCDC reference numbers are 1002281, 1002282 and 1002283, respectively. Copies of the data can be obtained, free of charge, on application to the CCDC, 12 Union Road, Cambridge CB2 1EZ, UK. Tel: +44-01223-762910; fax: +44-01223-336033; e-mail: deposit@ccdc.cam.ac.uk or http://www.ccdc.cam.ac.uk.

References

1 C. Metcalfe and J. A. Thomas, *Chem. Soc. Rev.,* 2003, **32**, 215-224.

2 M. Shakir, M. Azam, M. F. Ullah and S. M. Hadi, *J. Photoch. Photobio. B.,* 2011,**104**, 449-456.

3 S. Nafisi, A. A. Saboury, N. Keramat, J. F. Neault and H. A. Tajmir-Riahi, *J. Mol. Struct.,* 2007, 827, 35-43.

4 K. E. Erkkila, D. T. Odom and J. K. Barton, *Chem. Rev.,* 1999, **99**, 2777 -2795.

5 L.-N. Ji, X.-H. Zou and J.-G. Lin, *Coord. Chem. Rev.,* 2001, **216/217**, 513-536.

6 B. M. Zeglis, V. C. Pierre and J. K. Barton, *Chem. Commun.,* 2007, **44**, 4565-4579.

7 H.-L. Wu, J.-K. Yuan, Y. Bai, G.-L. Pan, H. Wang, J. Kong, X.-Y. Fan and H.-M. Liu, *Dalton Trans.,* 2012, **41**, 8829-8838.

8 C. O. Dietrich-Buchecker, J. Guilhem, J. M. Kern, C. Pascard and J. P. Sauvage, *Inorg. Chem.,* 1994, **33**, 3498-3502.

9 A. M. Bond, R. Colton, J. E. Kevekordes and P. Panagiotidou, *Inorg. Chem.,* 1987, **26**, 1430-1435.

10 P. L. Holland and W. B. Tolman, *J. Am. Chem. Soc.,* 2000, **122**, 6331-6332.

11 J. Velik, V. Baliharova, J. Fink-Gremmels, S. Bull, J. Lamka and L. Skalova, *Res. Vet. Sci.* 2004, **76**, 95-108.

12 J. M. Shin, Y. M. Cho, and G. Sachs, *J. Am. Chem. Soc.,* 2004, **126**, 7800-7811.

13 M. M. Ramla, M. A. Omar, H. Tokuda and I. El-Diwani, *Bioorg. Med. Chem.,* 2007, **15**, 6489-6496.

14 I. G. Safonov, D. A. Heerding, R. M. Keenan, A. T. Price, C. L. Erickson-Miller, C. B. Hopson, J. L. Levin, K. A. Lord, P. M. Tapley, *Bioorg. Med. Chem. Lett.* 2006, **16**, 1212-1216.

15 C.-M. Chang, M. V. Kulkarni, C.-H. Chen, C.-H. Wang and C.-M. Sun, *J. Comb. Chem.,* 2008, **10**, 466-474.

16 Z.-M. Wu, P. Rea and G. Wickham, *Tetrahedron Lett.,* 2000, **41,** 9871-9874.

17 A. D. Roy, S. Sharma, R. K. Grover, B. Kundu, and R. Roy, *Org. Lett.,* 2004, **6**, 4763-4766.

18 J.-A. Zhang, M. Pan, J.-Y. Zhang, H.-K. Zhang, Z.-J. Fan, B.-S. Kang and C.-Y. Su, *Polyhedron.,* 2009, **28**, 145-149.

19 H.-L. Wu, J.-K. Yuan, G.-L. Pan, Y.-H. Zhang, X.-L. Wang, F.-R. Shi, and X.-Y. Fan . *Journal of Photochemistry and Photobiology B: Biology.,* 2013, **122**, 37-44.

20 S. C. Yang and W. B. Tzeng, *Chemical Physics Letters.,* 2010, **501**, 6-10

21 H.-L. Wu, H.-C. Huang, J.-K. Yuan, F. Kou, G.-S. Chen, B.-B. Jia, Y. Yang and Y.-L. Lan, *Z. Naturforsch.,* 2010, **65b**, 1334-1340.

22 R. Bakshi and P. Mathur, *Inorganica Chimica Acta.,* 2010, **363**, 3477-3488.

23 F. Z. C. Fellah, J. P. Costes, C. Duhayon , J. C. Daran, and J. P. Tuchagues, *Polyhedron .,* 2010, 29, 2111-2119.

24 X.-F. Guo, Z-F. Li, C. Yue, G. Li, Y.-C. Gao and Y. Zhu, *Polyhedron.,* 2010, 29, 384-390.

25 H.-L. Wu, J.-K. Yuan, Y. Bai, G.-L. Pan, H. Wang and X.-B Shu, *Journal of Photochemistry and Photobiology B: Biology.,* 2012, **107**, 65-72.

26 H. Hioki, K. Matsuhita, M. Kubo, K. Harada, M. Kodama and Y. Fukuyama, *Tetrahedron.,* 2007, **63**, 11315-11324.

27 P. M. Bendale and C.-M. Sun, *J. Comb. Chem.,* 2002, **4**, 359-361.

28 M.-J. Lin and C.-M. Sun, *Synlett.,* 2004, **4**, 663-666.

29 Q.-Y. Yang, S.-R. Zheng, R. Yang, M. Pan, R. Cao and C.-Y. Su, *CrystEngComm.,*

2009, **11**, 680-685.

30 V. A. Blatov, L. Carlucci, G. Ciani and D. M. Proserpio, *CrystEngComm.,* 2004, **6**, 378-395.

31 Y.-S. Su, M.-J. Lin and C.-M. Sun, *Tetrahedron Lett.,* 2005, **46**, 177-180.

32 D. Kang, J. Seo, S. Y. Lee, J. Y. Lee, K. S. Choi and S. S. Lee, *Inorganic Chemistry Communications.,* 2007, **10**, 1425-1428.

33 N. Takagi and S. Sakaki, *Journal of American chemical society.,* 2012, **134**, 11749-11759.

34 N. M. Aghatabay, A. Neshat, T. Karabiyik, M. Somer, D. Haciu and B. Dulger, *Eur. J. Med. Chem.,* 2007, **42**, 205-213.

35 X.-P. Li, M. Pan, S.-R. Zheng, Y.-R. Liu, Q.-T. He, B.-S. Kang and C.-Y. Su *Crystal Growth & Design.,* 2007, **7**, 2481-2490.

36 H.-L. Wu, R.-R. Yun, K.-T.Wang, Ke Li, X.-C. Huang and Tao Sun, *Z. Anorg. Allg. Chem.,* 2010, **636**, 629-633.

37 Y.-C. Liu and Z.-Y. Yang, *Eur. J. Med. Chem.* 2009, **44**, 5080-5089.

38 C. Behrens, N. Harrit and P. E. Nielsen, *Bioconjugate Chem.* 2001, **12**, 1021-1027.

39 G.-L. Pan, Y.-C. Bai, H. Wang, J. Kong, F.-R. Shi, Y.-H. Zhang, X.-L. Wang and H.-L. Wu, *Z. Naturforsch.,* 2013, **68b**, 257-266.

40 S. Yellappa, J. Seetharamappa, L. M. Rogers, R. Chitta, R. P. Singhal and F. D'Souza, *Bioconjugate Chem.,* 2006, **17**, 1418-1425.

41 M. Shakir, M. Azam, M. F. Ullah, and S. M. Hadi, *J. Photoch. Photobio. B,* 2011, **104**, 449-456.

42 T. Ihara, S. Sueda, A. Inenaga, R. Fukuda and M. Takagi, *Supramol. Chem.,* 1997, **8**, 93-111.

43 X.-J. Xu, Z.-X. Xi, W.-Z. Chen and D.-Q. Wang, *J. Coord. Chem.* 2007, **60**, 2297-2308.

44 C. Metcalfe and J. A. Thomas, *Chem. Soc. Rev.* 2003, **32**, 215-224.

45 H. Chao and L.-N. Ji, *Bioinorg. Chem. Appl.* 2005, **3**, 15-28.

46 B. Peng, H. Chao, B. Sun, H. Li, F. Gao and L.-N. Ji, *J. Inorg. Biochem.* 2007, **101**, 404- 411.

47 M. Chauhan, K. Banerjee and F. Arjmand, *Inorg. Chem.* 2007, **46**, 3072- 3082.

48 D. Suh and J. B. Chaires, *Bioorg. Med. Chem.* 1995, **3**, 723-728.

49 K. Tsai, T. G. Hsu, K. M. Hsu, H. Cheng, T.-Y. Liu, C. F. Hsu and C.-W. Kong, *Free Radical Biol. Med.,* 2001, **31**, 1465-1472.

50 M. Xu, Y.-C. Zhang, Z.-H. Xu and Z.-Z. Zeng, *Inorganica Chimica Acta.,* 2012, **384**, 324-332.

51 S. Satyanarayana, J. C. Daborusak and J. B. Chaires, *Biochem.,* 1993, **32**, 2573-2584.

52 H.-L. Wu, B. Liu, F. Kou, F. Jia, J.-K. Yuan and Y. Bai, *Journal of the Chinese Chemical Society.,* 2012, **59**, 836-842.

53 R. Cariou, J. J. Chirinos, V. C. Gibson, G. Jacobsen, A. K. Tomov, G. J. P. Britovsek and A. J. P. White, *Dalton Trans.,* 2010, **39**, 9039-9045.

54 B.-D. Wang, Z.-Y. Yang, P. Crewdson and D.-Q. Wang, *J. Inorg. Biochem.,* 2007, **10**, 1492-1504.

55 C.-P. Tan, J. Liu, L.-M. Chen, S. Shi and L.-N. Ji, *J. Inorg. Biochem.* 2008, **102,** 1644-1653.

56 T.-R. Li, Z.-Y. Yang, B.-D. Wang and D.-D. Qin, *Eur J Med Chem*. 2008, **43**, 1688-1695.

57 J. I. Ueda, N. Saito, Y. Shimazu and T. Ozawa, *Arch. Biochem. Biophys*. 1996, **333**, 377-384.

58 M. Shakir, M. Azam, M. F. Ullah and S. M. Hadi, *J. Photochem. Photobiol. B.* 2011, **104**, 449-456.

59 C. C. Winterbourn, *Biochem. J.,* 1981, **198**, 125-131.

60 Z.-Y. Guo, R. E. Xing, S. Liu, H.-H. Yu, P.-B. Wang, C.-P. Li and P.-C. Li, *Bioorg. Med. Chem. Lett.,* 2005, **15**, 4600-4603.

61 X.-Y. Le, S.-R. Liao, X.-P. Liu and X.-L. Feng, *J. Coord. Chem.* 2006, **59**, 985-995.

62 Q.-H. Luo, Q. Lu, A.-B. Dai and L.-G. Huang, *J. Inorg.Biochem.,* 1993, **51**, 655-662.

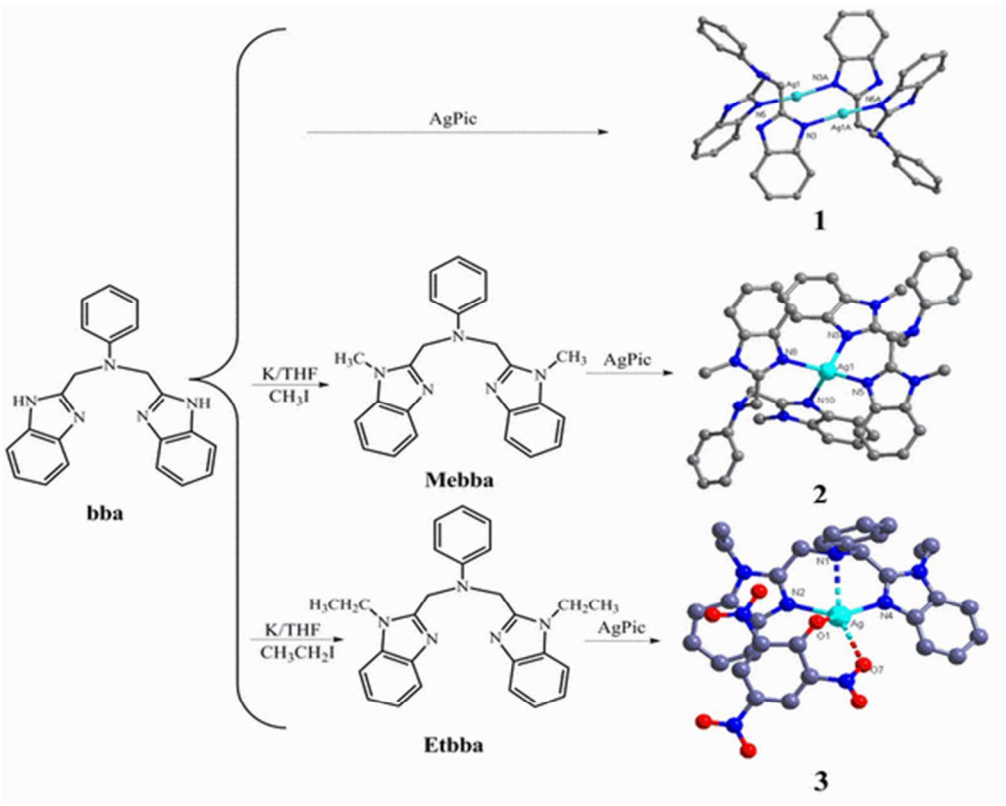

Scheme 1 Synthesis of ligands and complexes 1-3.
50x39mm (300 x 300 DPI)

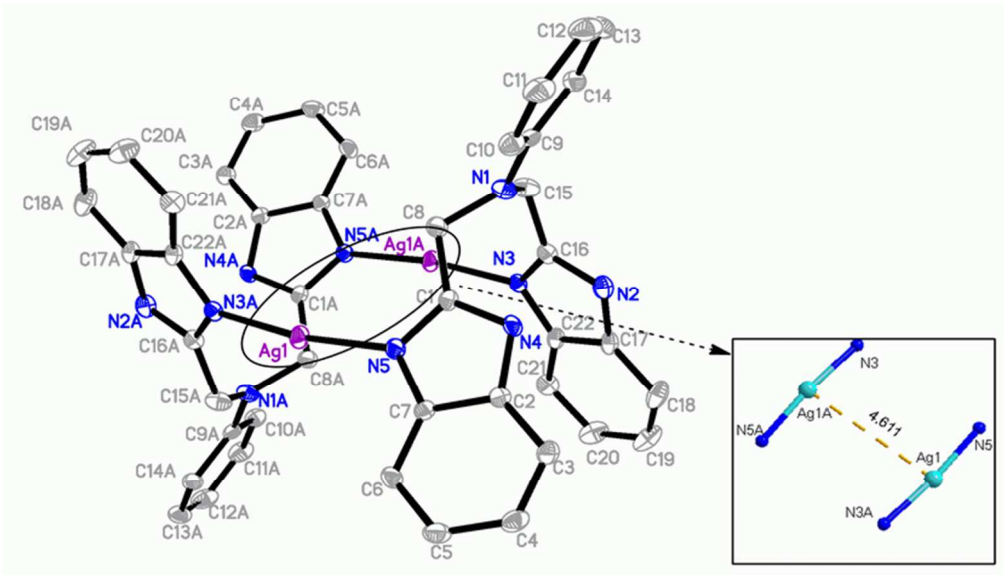

Fig.1 Molecular structure and atom-numberings of [Ag2(bba)2]2+ with hydrogen atoms omitted for clarity.
70x39mm (300 x 300 DPI)

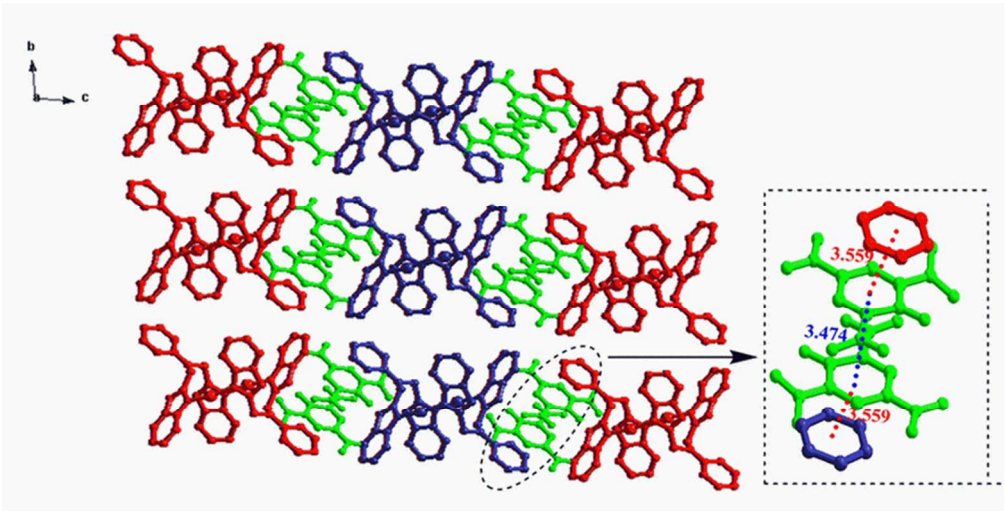

Fig. 2 2-D layer formed via π•••π interactions in complex 1 (different interactions are distinguished by different colors)
75x38mm (300 x 300 DPI)

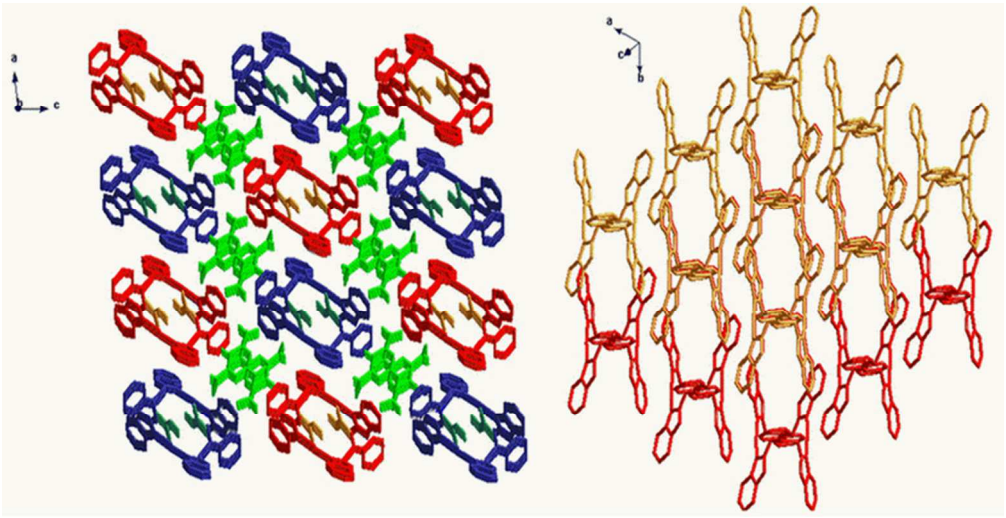

Fig. 3 3-D network of the [Ag2(bba)2]2+ cation.
70x35mm (300 x 300 DPI)

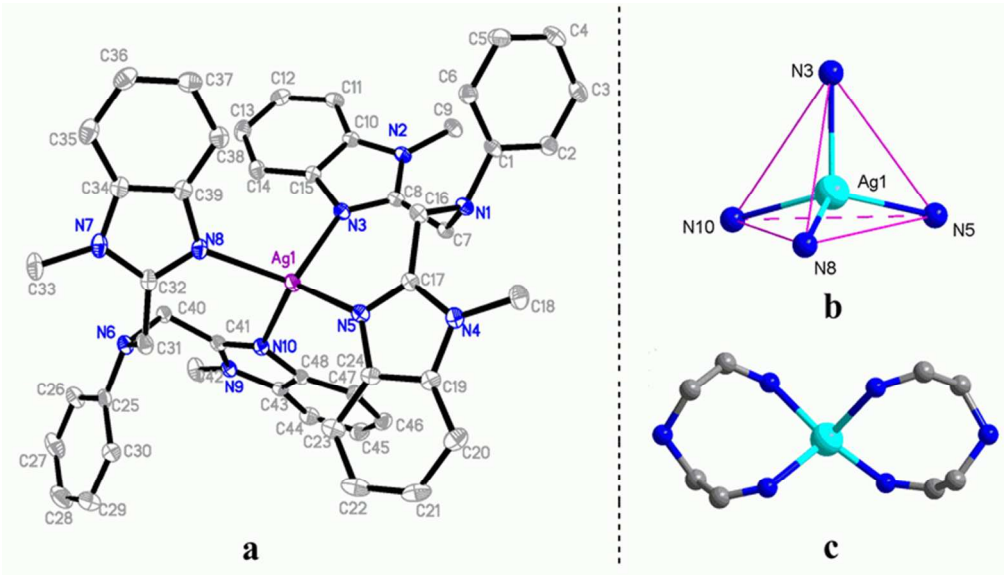

Fig. 4 Molecular structure of complex 2 with hydrogen atoms were omitted for clarity.
70x39mm (300 x 300 DPI)

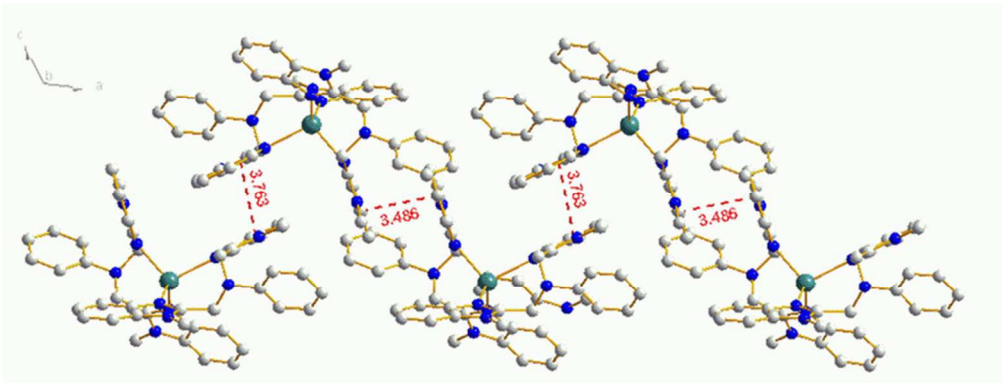

Fig. 5 The π•••π interactions and packing modes in complexes 2(H atoms are omitted).
78x29mm (300 x 300 DPI)

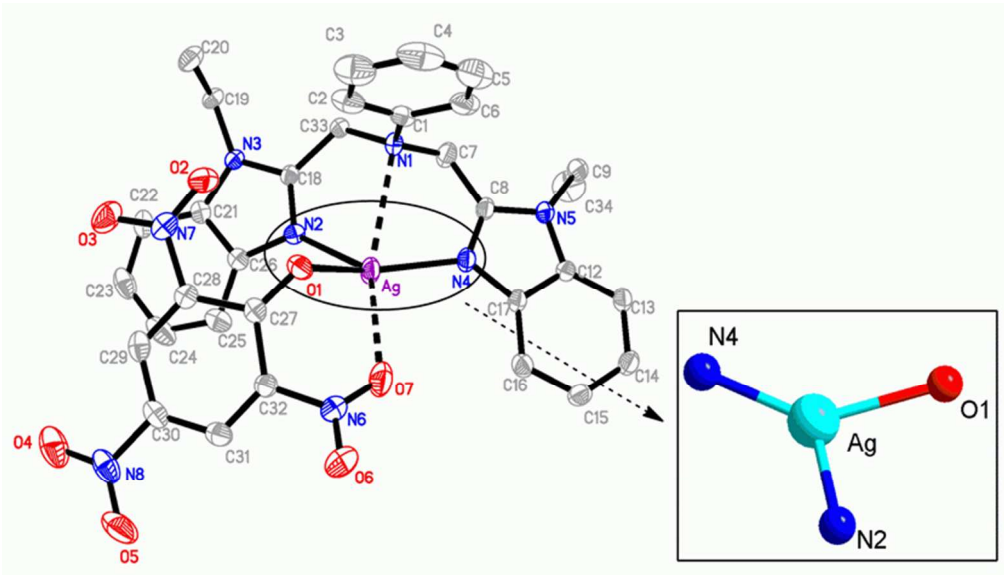

Fig. 6 The 1D chain structure of complex 3. The Ag-N(1) and Ag-O(7) weak coordination interaction are shown by an black broken line.
70x39mm (300 x 300 DPI)

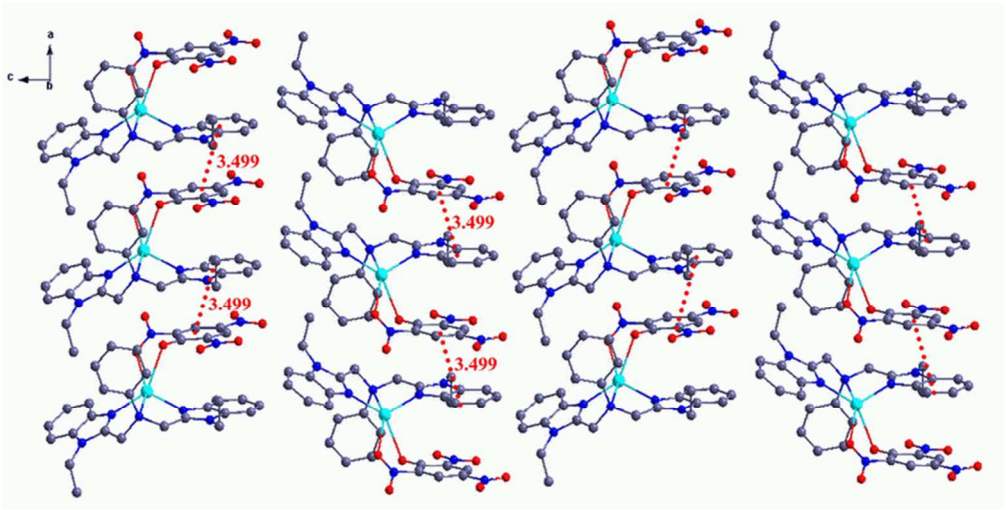

Fig. 7 2-D layer generated by the π•••π interactions and weak C–H•••O hydrogen bonding in the ac plane in complex 3 (for clarity, some atoms were omitted).
79x39mm (300 x 300 DPI)

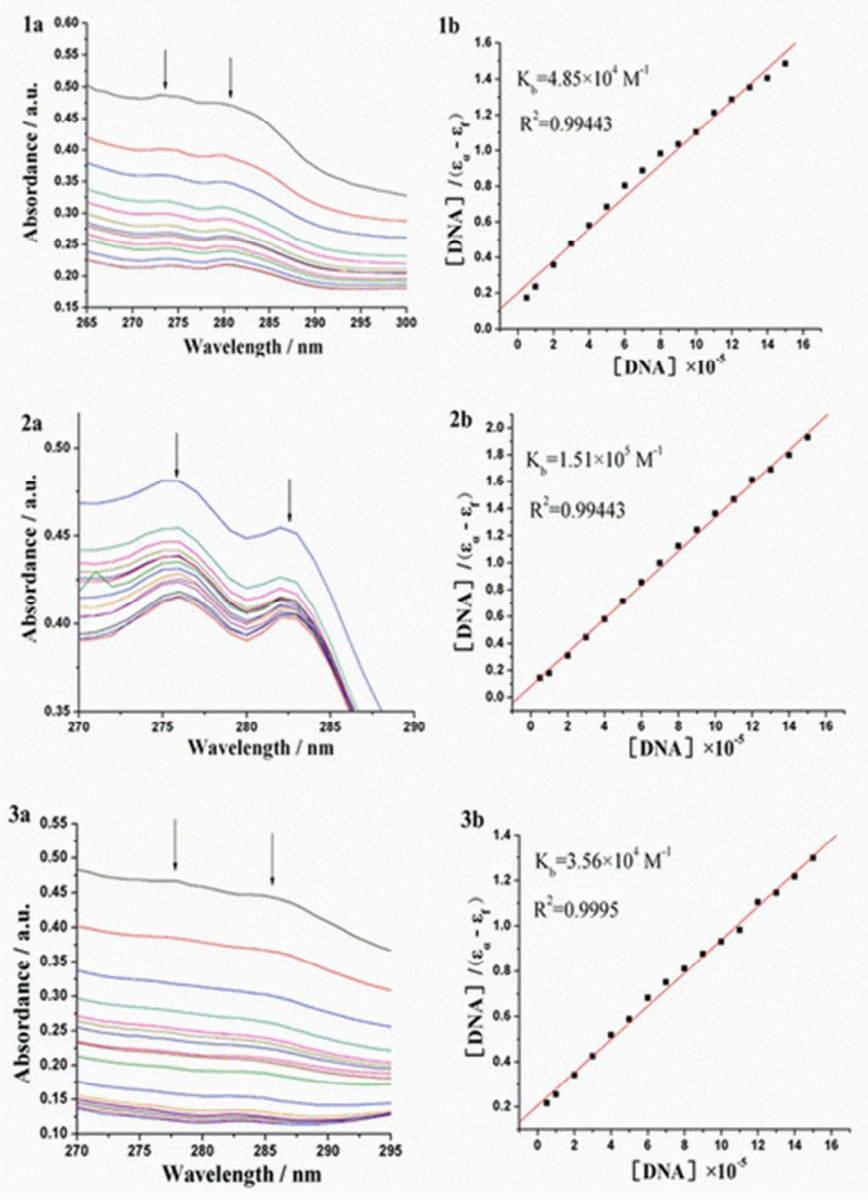

Fig. 8 Electronic spectra of (1a) 1, (2a) 2 and (3a) 3 in Tris–HCl buffer upon addition of CT-DNA. [Compound] =3 × 10−5 M−1, [DNA] = 3 × 10−5 M−1. Arrow shows the emission intensity changes upon increasing DNA concentration. Plots of [DNA]/(εa − εf) versus. [DNA] for the titration of (1b) 1, (2b) 2 and (3b) 3 with CT-DNA.
39x55mm (300 x 300 DPI)

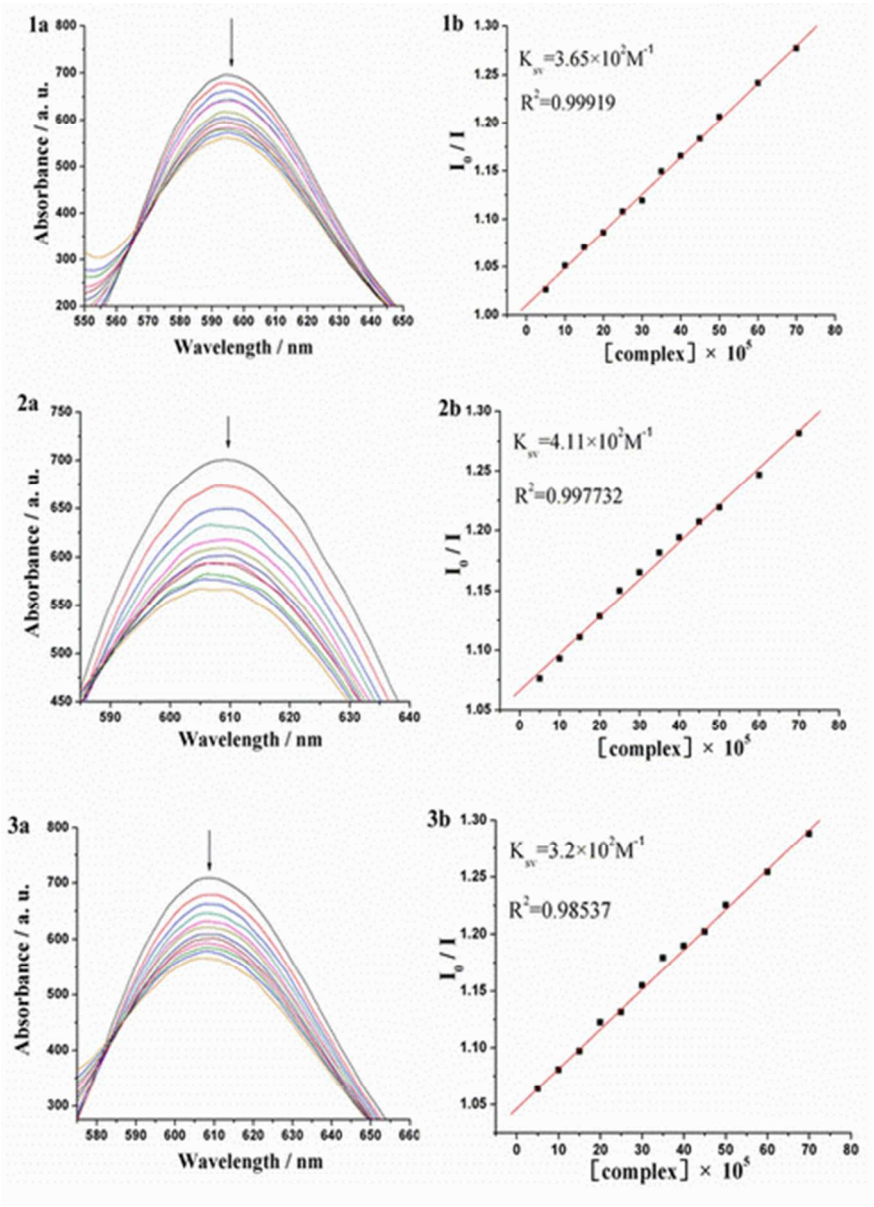

Fig. 9 Emission spectra of EB bound to CT-DNA in the presence of (1a) 1, (2a) 2 and (3a) 3; [Compound] = 3 × 10−5 M−1; λex = 520 nm. The arrows show the intensity changes upon increasing concentrations of the complexes. Fluorescence quenching curves of EB bound to CT-DNA by (1b) 1, (2b) 2 and (3b) 3. (Plots of I0/I versus [Complex]).
39x55mm (300 x 300 DPI)

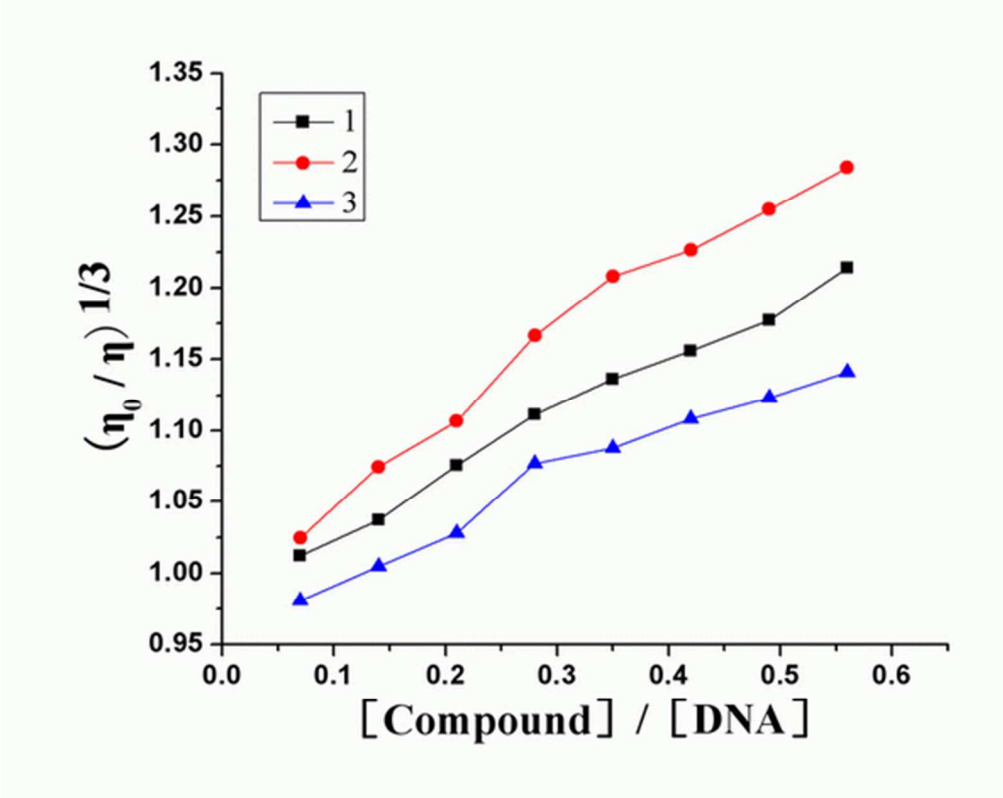

Fig. 10 Effect of increasing amounts of Ag(I) complexes on the relative viscosity of CT-DNA at 25.0 ± 0.1 °C.
50x39mm (300 x 300 DPI)

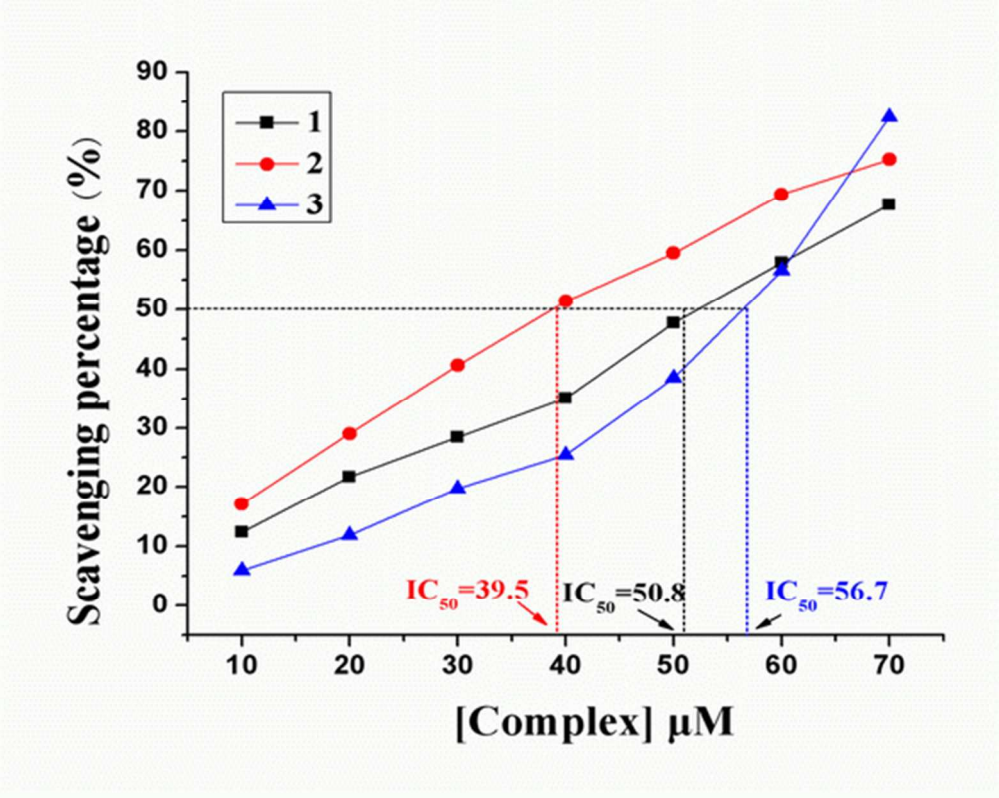

Fig. 11 The inhibitory effect of the three Ag(I) complexes on OH–• radicals; the suppression ratio increases with increasing concentration of the test compound.
50x39mm (300 x 300 DPI)

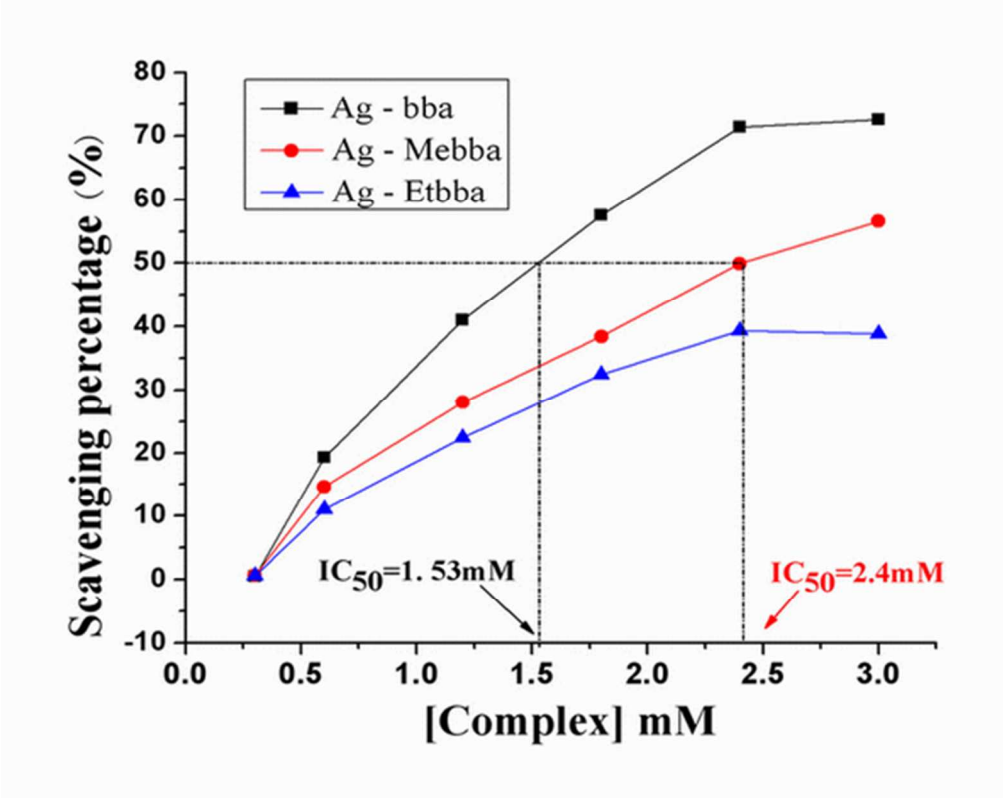

Fig. 12 Plots of scavenging percentage (%) versus concentration of the three Ag(I) complexes on superoxide radical.
50x39mm (300 x 300 DPI)

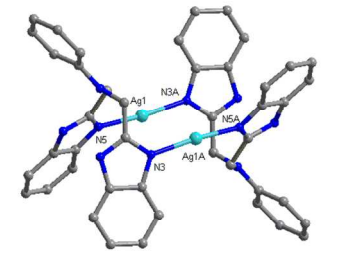

1

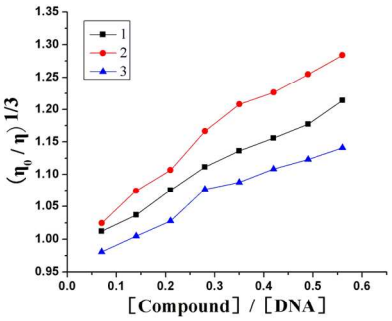

Measurements of DNA viscosity

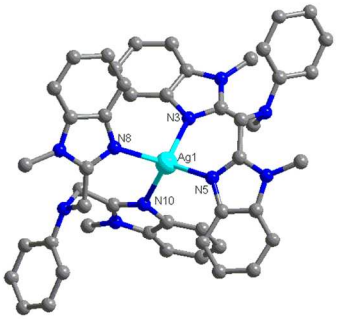

2

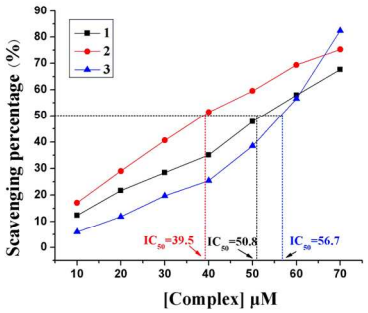

Hydroxyl radical scavenging activity

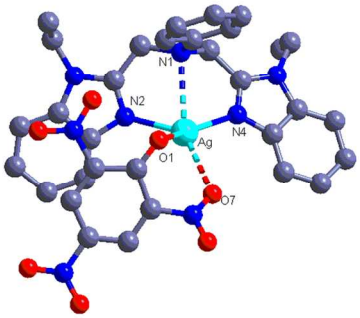

3

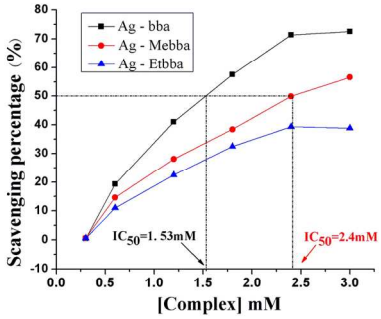

Superoxide radical scavenging activity

The cation of the complex 1 can be described as an overall chairlike conformation possessing a crystallographically imposed inversion center, owing to the strong interactions between the two Ag(I) ions themselves. The geometric structure of 2 may be treated as a distorted tetrahedron. In the complex 3, the coordination geometry around Ag(I) is best described as Y-shaped. DNA-binding of the Ag(I) complexes suggest that the three ligands and Ag(I) complexes bind to DNA in an intercalation mode. The DNA-binding affinities of these three complexes follow the order 2 > 1 > 3. Furthermore, the Ag(I) complexes have stronger ability of antioxidation for hydroxyl radical and superoxide radical.
142x189mm (300 x 300 DPI)